11532 *Inorg. Chem.* **2010**, *49*, 11532–11540
DOI: 10.1021/ic101687m

Inorganic Chemistry
Article

Single-Source Materials for Metal-Doped Titanium Oxide: Syntheses, Structures, and Properties of a Series of Heterometallic Transition-Metal Titanium Oxo Cages

Salvador Eslava,* Mary McPartlin, Richard I. Thomson, Jeremy M. Rawson, and Dominic S. Wright

Department of Chemistry, University of Cambridge, Lensfield Road CB2 1EW, Cambridge, United Kingdom

Received August 19, 2010

Titanium dioxide (TiO_2) doped with transition-metal ions (M) has potentially broad applications in photocatalysis, photovoltaics, and photosensors. One approach to these materials is through controlled hydrolysis of well-defined transition-metal titanium oxo cage compounds. However, to date very few such cages have been unequivocally characterized, a situation which we have sought to address here with the development of a simple synthetic approach which allows the incorporation of a range of metal ions into titanium oxo cage arrangements. The solvothermal reactions of $Ti(OEt)_4$ with transition-metal dichlorides ($M^{II}Cl_2$, M = Co, Zn, Fe, Cu) give the heterometallic transition-metal titanium oxo cages $[Ti_4O(OEt)_{15}(MCl)]$ [M = Co (**2**), Zn (**3**), Fe (**4**), Cu (**5**)], having similar $MTi_4(\mu_4\text{-O})$ structural arrangements involving ion pairing of $[Ti_4O(OEt)_{15}]^-$ anion units with MCl^+ fragments. In the case of the reaction of $MnCl_2$, however, two Mn^{II} ions are incorporated into this framework, giving the hexanuclear $Mn_2Ti_4(\mu_4\text{-O})$ cage $[Ti_4O(OEt)_{15}(Mn_2Cl_3)]$ (**6**) in which the MCl^+ fragments in **2**−**5** are replaced by a $[ClMn(\mu\text{-Cl})MnCl]^+$ unit. Emphasizing that the nature of the heterometallic cage is dependent on the metal ion (M) present, the reaction of $Ti(OEt)_4$ with $NiCl_2$ gives $[Ti_2(OEt)_9(NiCl)]_2$ (**7**), which has a dimeric $Ni(\mu\text{-Cl})_2Ni$ bridged arrangement arising from the association of $[Ti_2(OEt)_9]^-$ ions with $NiCl^+$ units. The syntheses, solid-state structures, spectroscopic and magnetic properties of **2**−**7** are presented, a first step toward their applications as precursor materials.

Titanium oxo cages of the type $[Ti_xO_y(OR)_z(L)_w]$ have been used as nanobuilding blocks for the formation of hybrid organic−inorganic materials, from which materials with enhanced mechanical, thermal, or photochromic properties have been obtained.[1−12] Bearing in mind the extensive applications of titanium dioxide (TiO_2) itself,[13] there are likely in the future to be many applications for hybrid materials containing Ti_xO_y cores in photovoltaic, electrochromic, photocatalytic, and sensing devices. It is well-known that doping of TiO_2 with nonmetals (E), such as N and B, results in low band-gap materials with visible light activity ['TiO_2(E)'],[14,15] with potential future applications in the photodegradation of air or water pollutants. In this regard, the applications of TiO_2 may well be expanded if it is doped with transition metals (M) that absorb in the visible

*Corresponding author. E-mail: se296@cam.ac.uk.

(1) Rozes, L.; Steunou, N.; Fornasieri, G.; Sanchez, C. *Monatsh. Chem.* **2006**, *137*, 501.
(2) Sanchez, C.; Rozes, L.; Ribot, F.; Laberty-Robert, C.; Grosso, D.; Sassoye, C.; Boissiere, C.; Nicole, L. *C. R. Chim.* **2010**, *13*, 3.
(3) Fornasieri, G.; Rozes, L.; Le Calve, S.; Alonso, B.; Massiot, D.; Rager, M. N.; Evain, M.; Boubekeur, K.; Sanchez, C. *J. Am. Chem. Soc.* **2005**, *127*, 4869.
(4) Mosset, A.; Galy, J. *C. R. Acad. Sci., Ser I.* **1988**, *307*, 1747.
(5) Schmid, R.; Mosset, A.; Galy, J. *J. Chem. Soc., Dalton Trans.* **1991**, 1999.
(6) Le Calve, S.; Alonso, B.; Rozes, L.; Sanchez, C.; Rager, M. N.; Massiot, D. *C. R. Chim.* **2004**, *7*, 241.
(7) Rozes, L.; Fornasieri, G.; Trabelsi, S.; Creton, C.; Zafeiropoulos, N. E.; Stamm, M.; Sanchez, C. *Prog. Solid State Chem.* **2005**, *33*, 127.
(8) Bocchini, S.; Fornasieri, G.; Rozes, L.; Trabelsi, S.; Galy, J.; Zafeiropoulos, N. E.; Stamm, M.; Gerard, J. F.; Sanchez, C. *Chem. Commun.* **2005**, *20*, 2600.
(9) Trabelsi, S.; Janke, A.; Hässler, R.; Zafeiropoulos, N. E.; Fornasieri, G.; Bocchini, S.; Rozes, L.; Stamm, M.; Gérard, J. F.; Sanchez, C. *Macromolecules* **2005**, *38*, 6068.
(10) Shubert, U.; Gao, Y.; Kogler, F. R. *Prog. Solid State Chem.* **2007**, *35*, 161.
(11) Moraru, B.; Husing, N.; Kickelbick, G.; Schubert, U.; Fratzl, P.; Peterlik, H. *Chem. Mater.* **2002**, *14*, 2732.
(12) Eslava, S.; Papageorgiou, A. C.; Beaumont, S. K.; Kyriakou, G.; Wright, D. S.; Lambert, R. M. *Chem. Mater.* **2010**, *22*, 5174.
(13) Chen, X.; Mao, S. S. *Chem. Rev.* **2007**, *107*, 2891.
(14) (a) Linsebigler, A. L.; Lu, G.; Yates, J. T. *Chem. Rev.* **1995**, *95*, 735. (b) Asahi, R.; Morikawa, T.; Ohwaki, T.; Aoki, K.; Taga, Y. *Science* **2001**, *293*, 269. (c) Sakthivel, S.; Janczarek, M.; Kisch, H. *J. Phys. Chem. B* **2004**, *108*, 19384. (d) Sakthivel, S.; Kisch, H. *ChemPhysChem* **2003**, *4*, 487. (e) Huang, X. H.; Tang, Y. C.; Hu, C.; Yu, H. Q.; Chen, C. S. *J. Environ. Sci.* (*Beijing, China*) **2005**, *17*, 562. (f) Kobayakawa, K.; Murakami, Y.; Sato, Y. *J. Photochem. Photobiol., A* **2005**, *170*, 177. (g) Livraghi, S.; Votta, A.; Paganini, M. C.; Giamello, E. *Chem. Commun.* **2005**, *4*, 498. (h) Wang, Z. P.; Cai, W. M.; Hong, X. T.; Zhao, X. L.; Xu, F.; Cai, C. G. *Appl. Catal., B* **2005**, *57*, 223. (i) In, S.; Orlov, A.; Garcia, F.; Tikhov, M.; Wright, D. S.; Lambert, R. M. *Chem. Commun.* **2006**, 4236.
(15) (a) Grey, I. E.; Li, C.; MacRae, D. M.; Bursill, L. A. *J. Solid State Chem.* **1996**, *127*, 240. (b) Moon, S. C.; Mametsuka, H.; Tabata, S.; Suzuki, E. *Catal. Today* **2000**, *58*, 125. (c) Zhao, W.; Ma, W. H.; Chen, C.; Zhao, J. C.; Shuai, Z. G. *J. Am. Chem. Soc.* **2004**, *126*, 4782. (d) Chen, D.; Yang, D.; Wang, Q.; Jiang, Z. Y. *Ind. Eng. Chem. Res.* **2006**, *45*, 4110. (e) In, S.; Orlov, A.; Berg, R.; Garcia, F.; Pedrosa-Jimenez, S.; Tikhov, M. S.; Wright, D. S.; Lambert, R. M. *J. Am. Chem. Soc.* **2007**, *129*, 13790.

Published on Web 11/18/2010

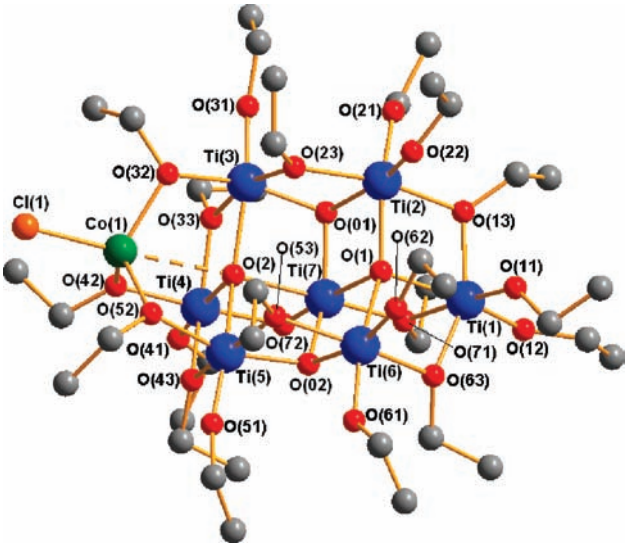

Figure 1. Structure of the heterometallic complex $[Ti_7O_5(OEt)_{19}(CoCl)]$ (**1**). H-atoms and the minor components of disorder in some of the EtO groups are omitted for clarity.

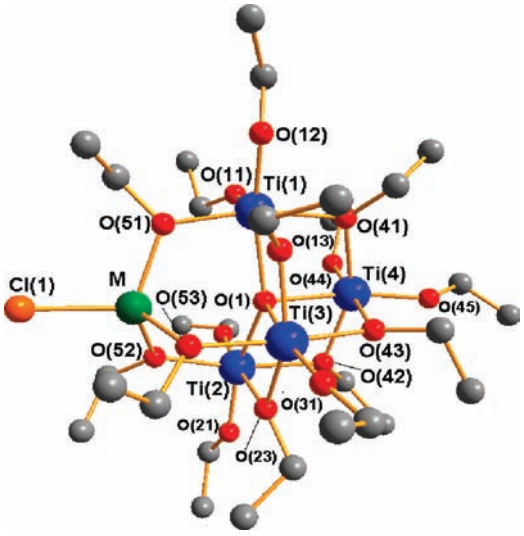

Figure 2. Structure of the heterometallic complexes $[Ti_4O(OEt)_{15}(CoCl)]$ (**2**), $[Ti_4O(OEt)_{15}(ZnCl)]$ (**3**), and $[Ti_4(OEt)_{15}(FeCl)]$ (**4**) [M = Co(1), Zn(1), or Fe(1)]. H-atoms and the minor disorder components in some of the EtO groups are omitted for clarity. Selected bond lengths (Å) and angles (°): Within **2**−**4**, Ti−OEt(terminal) range 1.769(2)−1.829(10), Ti−(μ_2-OEt) range 1.943(9)−2.142(11), Ti−μ_2-O(51, 52, 53) range 1.971-(3)−2.002(12), Ti−O(1) range 2.056(9)−2.163(3); Ti−O(1)−Ti range 96.0(1)−150.7(1), Ti−(μ_2-OEt)−Ti range 102.9(5)−106.5(1). **2** (M = Co), Co−Cl(1) 2.251(1), Co−μ_2-O(51, 52, 53) range 1.956(3)−1.969(3), Co-(1)···O(1) 2.934(3), O−Co−O range 101.9(1)−118.4(1), Cl(1)−Co−O range 108.6(1)−114.9(1), Co−O−Ti range 111.8(1)−119.5(1). **3** (M = Zn), Zn−Cl(1) 2.210(5), Zn−μ_2-O(51, 52, 53) range 1.944(13)−1.961(10), Zn···O(1) 3.062(12), O−Zn−O range 100.6(4)−111.8(5), Cl(1)−Zn−O range 111.4(3)−117.7(5), Zn−O−Ti range 114.5(8)−124.6(4). **4** (M = Fe), Fe−Cl(1) 2.277(2), Fe−μ_2-O(51, 52, 53) range 1.978(4)−1.998(3), Fe-(1)···O(1) 2.938(4), O−Fe−O range 97.8(1)−123.6(2), Cl(1)−Fe−O range 106.6(1)−117.1)(1), Fe−O−Ti range 112.8(1)−120.4(2).

region, which are therefore likely to mediate the photochemical formation of holes and electrons for oxidation and reduction of organic pollutant molecules. Indeed, this potential has already been demonstrated in the doping of bulk TiO_2 with transition-metal ions, such as Co, Fe and Cu.[16−18]

An obvious route by which transition-metal-doped TiO_2 could be obtained is through controlled hydrolysis and/or condensation of heterometallic transition-metal cage compounds, potentially allowing greater control of the stoichiometry of the transition-metal ions and more uniform distribution of the transition-metal ions within TiO_2.[19,20] Examples of heterometallic transition-metal cages containing titanium have been previously reported, but new routes and different stoichiometries are necessary to provide wider access to a variety of doped TiO_2 materials.[21,22] In this context, we have recently communicated the formation of the octanuclear and pentanuclear Co^{II}-doped Ti_xO_y complexes $[Ti_7O_5(OEt)_{19}(CoCl)]$ (**1**) and $[Ti_4O(OEt)_{15}(CoCl)]$ (**2**) (Figures 1 and 2, respectively).[23] These cages are key building blocks for transition-metal-doped bulk TiO_2 as well as advanced hybrid materials (i.e., by cross-linking of the molecular building blocks with organic linkers). Unlike undoped Ti_xO_y cages of this type which absorb in the UV only, the new Co-doped cages absorb radiation in the UV and visible light regions. In this paper, we demonstrate that a new approach (used initially in the preparation of **2**) can be generalized to allow access to a broad range of related heterometallic transition-metal titanium oxo cages. The new pentanuclear cages $[Ti_4O(OEt)_{15}(ZnCl)]$ (**3**), $[Ti_4O(OEt)_{15}(FeCl)]$ (**4**), and $[Ti_4O(OEt)_{15}(CuCl)]$ (**5**) (all structurally related to **2**) are reported, along with the hexanuclear compounds $[Ti_4O(OEt)_{15}(Mn_2Cl_3)]$ (**6**) and $[Ti_2(OEt)_9(NiCl)]_2$ (**7**). In addition, the spectroscopic properties and the variable-temperature magnetic behavior of **2**−**7** have been investigated.

Experimental Section

Synthetic Procedures and Characterization of 2−7. Strict inert atmospheric conditions and a dry, O_2-free atmosphere were used throughout all of the syntheses. Ultrapure, anhydrous salts ($M^{II}Cl_2$) and $TiOEt_4$ were acquired from Aldrich and Alfa-Aesar chemical companies. Solvents used were dried by distillation over Mg turnings (EtOH) and sodium/benzophenone (toluene and tetrahydrofuran). Drying of reactants was necessary to avoid the formation of $[Ti_7O_4(OEt)_{20}]$ cages as a byproduct. Twenty-three mL capacity Teflon-lined autoclaves (model 4749, Parr) were used for all experiments. Autoclaves were heated using a Binder ED53 53 L oven with natural convection. All analytical and spectroscopic samples were prepared inside a Saffron Scientific (type β) glovebox, equipped with a closed loop recirculation system for the removal of

(16) Anpo, M.; Takeuchi, M. *J. Catal.* **2003**, *216*, 505.
(17) Morikawa, T.; Ohwaki, T.; Suzuki, K. I.; Moribe, S.; Tero-Kubota, S. *Appl. Catal., B* **2008**, *83*, 56.
(18) Yamashita, H.; Harada, M.; Misaka, K.; Takeuchi, M.; Neppolian, B.; Anpo, M. *J. Photochem. Photobiol., A* **2002**, *148*, 257.
(19) (a) Musgraves, J. D.; Potter, B. G.; Boyle, T. J. *J. Mater. Res.* **2009**, *24*, 3372. (b) Musgraves, J. D.; Potter, B. G.; Boyle, T. J. *Opt. Lett.* **2008**, *33*, 1306. (c) Musgraves, J. D.; Potter, B. G.; Sewell, R. M.; Boyle, T. J. *J. Mater. Res.* **2007**, *22*, 1694. (d) Hernandez-Sanchez, B. A.; Boyle, T. J.; Baros, C. M.; Brewer, L. N.; Headley, T. J.; Tallant, D. R.; Rodriguez, M. A.; Tuttle, B. A. *Chem. Mater.* **2007**, *19*, 1459. (e) Boyle, T. J.; Tyner, R. P.; Alam, T. M.; Scott, B. L.; Ziller, J. W.; Potter, B. G. *J. Am. Chem. Soc.* **1999**, *121*, 12104. (f) Boyle, T. J.; AlShareef, H. N. *J. Mater. Sci.* **1997**, *32*, 2263. (g) Boyle, T. J.; Dimos, D.; Schwartz, R. W.; Alam, T. M.; Sinclair, M. B.; Buchheit, C. D. *J. Mater. Res.* **1997**, *12*, 1022.
(20) Seisenbaeva, G. A.; Kessler, V. G.; Pazik, R.; Strek, W. *Dalton Trans.* **2008**, 3412–3421.
(21) (a) Kessler, V. G. *Chem. Commun.* **2003**, 1213. (b) Seisenbaeva, G. A.; Mallah, T.; Kessler, V. G. *Dalton Trans.* **2010**, *39*, 7774. (c) Kessler, V. G.; Gohil, S.; Parola, S. *Dalton Trans.* **2003**, 544. (d) Seisenbaeva, G. A.; Gohil, S.; Kessler, V. G. *Inorg. Chem.* **2004**, *7*, 18.
(22) Clegg, W.; Elsegood, M. R. J.; Errington, R. J.; Havelock, J. *J. Chem. Soc., Dalton Trans.* **1996**, 681.
(23) Eslava, S.; Hengesbach, F.; Mcpartlin, M.; Wright, D. S. *Chem. Commun.* **2010**, *46*, 4701.

moisture and oxygen (operating at ca. 0.1−0.5 vppm O_2). Melting points were recorded on a standard melting point apparatus. IR spectra were recorded as Nujol mulls using a Perkin-Elmer 1710 FT spectrophotometer and CsI windows. Both carbon and hydrogen analyses were done by using a Perkin-Elmer 240 Elemental analyzer, and chlorine analysis was done by titration against silver nitrate using a radiometer TTT85 titrator. NMR samples were dissolved in 0.75 mL of dry, C_6D_6 (or C_4D_8O for **6**) in the glovebox in Wilmad 528PP NMR tubes and were sealed with tight-fitting caps and parafilm prior to immediate acquisition of the spectra. Standard (1D) ^1H and ^{13}C NMR and 2D $^1H-^1H$ correlation spectroscopy (COSY) spectra were recorded using a Bruker Avance Cryo Ultrashield 500 MHz spectrometer (500.05 MHz for ^1H, 125.7 MHz for ^{13}C), with both being referenced to the solvent peaks. $^{13}C-^1H$ heteronuclear single-quantum coherence (HSQC) 2D spectra were measured on a Bruker Avance Cryo Ultrashield 500 MHz spectrometer (for ^{13}C resonance) and a Bruker Avance 700 MHz Ultrashield with TXI Cryoprobe (for ^1H resonance). Variable-temperature magnetic measurements on polycrystalline samples (ca. 20−50 mg) of **2** and **4**−**7** were made in the region of 5−300 K in an applied field of 2500 G. Corrections were applied for sample diamagnetism and the sample holder.

Synthesis of $[Ti_4O(OEt)_{15}(CoCl)]$ (2). Details of this synthesis and the characterization were previously described in ref 23.

Synthesis of $[Ti_4O(OEt)_{15}(ZnCl)]$ (3). Titanium ethoxide (7.00 mL, 33.4 mmol), zinc(II) chloride (284 mg, 2.09 mmol), and anhydrous ethanol (7.00 mL, 120 mmol) were placed in a Teflon-lined autoclave and heated at 150 °C for 1 day. After slow cooling overnight to room temperature, crystals of **2** were isolated from the reactant solution, rinsed with dry ethanol, and dried under vacuum (1.0 g, 49% yield, with respect to $ZnCl_2$ supplied). IR (1500−400 cm^{-1}): ν/cm^{-1} = 1118(s), 1071(s), 1046(s), 914(m), 894(m), 610(s), 560(s), 441(w). Elemental analysis (%) calcd for $C_{30}H_{75}ClZnO_{16}Ti_4$: C, 36.6; H, 7.7; Cl, 3.6; found C, 36.0; H, 7.6; Cl, 3.9. Melting point: 160 °C. ^1H NMR (C_6D_6, δ ppm): collection of multiplets in the ranges 4.8−4.1 (30H in $-OCH_2CH_3$) and 1.8−1.1 (45 in $-OCH_2CH_3$). ^{13}C NMR (C_6D_6, δ ppm): 72.6, 72.4, 71.9, 71.5, 69.7, 68.6, 68.5, 67.9, 67.1 (15 $-OCH_2CH_3$); 20.3, 20.1, 19.6, 19.3 (including a shoulder), 19.0. 18.9, 18.7, 18.4 (15 $-OCH_2CH_3$).

Synthesis of $[Ti_4O(OEt)_{15}(FeCl)]$ (4). Titanium ethoxide (7.00 mL, 33.4 mmol), iron(II) chloride (2.09 mmol, 264 mg), and anhydrous ethanol (7.00 mL, 120 mmol) were placed in a Teflon-lined autoclave and heated at 150 °C for 1 day. After slow cooling overnight to room temperature, the subsequent evaporation of ethanol and crystallization in dry toluene (10 mL) at −14 °C produced brown crystals of **4** (1.4 g, 68% yield, with respect to $FeCl_2$ supplied). Experiments with $FeCl_3$ instead of $FeCl_2$ showed that **4** is also produced (in lower yield). IR (1500−400 cm^{-1}): ν/cm^{-1} = 1116(s), 1066(s), 1046(s), 915(m), 894(m), 610(s), 533(s), 428(w). Elemental analysis (%) calcd for $C_{30}H_{75}ClFeO_{16}Ti_4$: C, 37.0; H, 7.8; Cl, 3.6; found C, 37.2; H, 7.7; Cl, 3.3. Melting point: 110 °C. ^1H NMR (C_6D_6, δ ppm): collection of multiplets in the ranges 4.8−4.1 ($-OCH_2CH_3$) and 1.8−1.4 ($-OCH_2CH_3$). ^{13}C NMR (C_6D_6, δ ppm): collection of broad and narrow resonances in the range 71.5−67.5 ($-OCH_2CH_3$); collection of broad and narrow resonances in the range 20.5−16.0 ($-OCH_2CH_3$).

Synthesis of $[Ti_4O(OEt)_{15}(CuCl)]$ (5). The use of copper(II) chloride and the same stoichiometry and protocol as used for **2**−**4** resulted in the final isolation of a brownish liquid that does not crystallize at low temperatures. Higher Cu:Ti ratios resulted in a more brownish liquid. Subsequently, a lower heating temperature was used. The highest yield of **5** was obtained using a 5:1 ratio of $Ti(OEt)_4$:$CuCl_2$; titanium ethoxide (7.00 mL, 33.4 mmol), copper(II) chloride (842 mg, 6.26 mmol), and anhydrous ethanol (5.00 mL, 85.7 mmol) were placed in a Teflon-lined autoclave and heated at 100 °C for 1 day. After slow cooling overnight to room temperature, the subsequent evaporation of ethanol and crystallization from 5 mL of dry tetrahydrofuran (THF) at −14 °C produced light-blue crystals of **5** (in 30% yield, on the basis of $CuCl_2$ supplied). Using a range of other stoichiometries, **5** is also formed: [$Ti(OEt)_4$: $CuCl_2$; 15:1 (3%) or 7:1 (14%)]. IR (1500−400 cm^{-1}): ν/cm^{-1} = 1135(s), 1101(s), 1067(s), 1050(s), 917(m), 894(m), 805(w), 596(s), 553(s), 488(m), 446(w). Elemental analysis (%) calcd for $C_{30}H_{75}ClCuO_{16}Ti_4$: C, 36.7; H, 7.7; Cl, 3.6; found C, 36.6; H, 7.6; Cl, 4.0. Melting point: 95 °C. ^1H NMR (C_6D_6, δ ppm): collection of multiplets in the ranges 5.1−4.2 ($-OCH_2CH_3$) and 2.0−1.1 ($-OCH_2CH_3$). ^{13}C NMR (C_6D_6, δ ppm): collection of broad and narrow resonances in the range 72.0−70.0 ($-OCH_2CH_3$); collection of overlapping resonances in the range 20.0−18.0 ($-OCH_2CH_3$).

Synthesis of $[Ti_4O(OEt)_{15}(Mn_2Cl_3)]$ (6). Titanium ethoxide (7.00 mL, 33.4 mmol), manganese(II) chloride (263 mg, 2.09 mmol), and anhydrous ethanol (7.00 mL, 120 mmol) were placed in a Teflon-lined autoclave and heated at 150 °C for 1 day. After slow cooling overnight to room temperature, subsequent partial evaporation of ethanol and crystallization in 15 mL of dry THF at −14 °C pale-yellow crystals of **6**·(**1/2EtOH**)·(**1/2THF**) were formed. Isolation and drying under vacuum (0.1 mbar, 60 min) of the crystals resulted in desolvated crystals of **6** (0.7 g, 62% yield with respect to $MnCl_2$ supplied). IR (1500−400 cm^{-1}): ν/cm^{-1} = 1115(s), 1075(s), 1042(s), 934(w), 894(s), 804(w), 616(w), 587(s), 554(s), 494(m), 443(w). Elemental analysis (%) calcd for $C_{30}H_{75}Cl_3Mn_2O_{16}Ti_4$: C, 32.8; H, 6.9; Cl, 9.7; found C, 32.7; H, 6.8; Cl, 9.8. Melting point: 110 °C. ^1H NMR (C_4D_8O, δ ppm): collection of multiplets in the ranges 4.8−4.1 ($-OCH_2CH_3$) and 1.8−1.0 ($-OCH_2CH_3$). ^{13}C NMR (C_4D_8O, δ ppm): collection of overlapping resonances in the range 75.0−58.0 ($-OCH_2CH_3$ and THF solvent); collection of overlapping resonances in the range 30.0−18.0 ($-OCH_2CH_3$ and THF solvent).

Synthesis of $[Ti_2(OEt)_9(NiCl)]_2$ (7). Titanium ethoxide (7.00 mL, 33.4 mmol), nickel(II) chloride (271 mg, 2.09 mmol), and anhydrous ethanol (7.00 mL, 120 mmol) were placed in a Teflon-lined autoclave and heated at 150 °C for 1 day. Subsequent evaporation of ethanol and crystallization in dry toluene (5 mL) at −14 °C produced dark-yellow crystals of **7** (0.50 g, 40% yield, with respect to $NiCl_2$ supplied). The same product and yield is obtained with a Ti: Ni ratio of 8:1. IR (1500−400 cm^{-1}): ν/cm^{-1} = 1274(w), 1147(s), 1098(s), 1070(s), 1046(s), 921(m), 899(m), 882(m), 600(s), 515(m), 435(w). Elemental analysis (%) calcd for $C_{36}H_{90}Cl_2Ni_2O_{18}Ti_4$: C, 36.3; H, 7.6; Cl, 6.0; found C, 35.9; H, 7.5; Cl, 6.5. Melting point: 170 °C. ^1H NMR (C_6D_6, δ ppm): collection of multiplets in the ranges 5.3−4.0 ($-OCH_2CH_3$) and 2.0−0.2 ($-OCH_2CH_3$). ^{13}C NMR (C_6D_6, δ ppm): collection of broad and narrow resonances in the range 74.0−70.0 ($-OCH_2CH_3$); collection of broad and narrow resonances in the range 20−18 ($-OCH_2CH_3$).

X-ray Crystallographic Studies of 3−5, 6·(1/2EtOH)·(1/2THF), and 7. Crystallographic data were collected on a Nonius Kappa CCD device equipped with an Oxford Cryostream low-temperature cooling device (λ = 0.71073 Å). Wet crystals were mounted using a perfluorocarbon oil which freezes at low temperature.[24] The structures were solved and refined by full matrix least-squares on F^2 using the SHELXTL program,[25] with anisotropic displacement parameters for all full occupancy atoms. All crystals diffracted relatively weakly due to considerable disorder of the carbon atoms of the −OEt ligands which had relatively high-displacement parameters. The disorder was resolved into two components for each of 4 C-atoms in (**3**), 6 in (**4**) and (**6**), 12 in (**5**), and 15 in (**7**); the average major occupancy factors (%) were 60 (**3**), 62 (**4**), 67 (**5**), 66 (**6**), and 64 (**7**). Half

(24) Kottke, T.; Stalke, D. *J. Appl. Crystallogr.* **1993**, *26*, 615.
(25) Sheldrick, G. M. *SHELXTL*, version 6.10; Bruker AXS Inc.: Madison, Wisconsin, 2000.

Scheme 1. Formation of the Anticipated Product $[Ti_2(OEt)_9(CoCl)]^a$

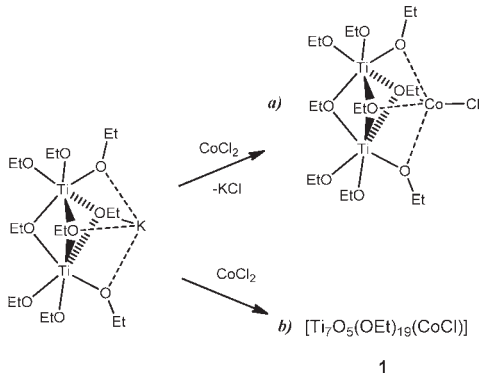

[a] Formation via route (a) and the product isolated from the reaction via route (b), the heterometallic Co−titanium oxo complex $[Ti_7O_5(OEt)_{19}(CoCl)]$ (**1**).

molecules of solvate THF and EtOH were located near the inversion center in the crystals of **6**·(**1/2EtOH**)·(**1/2THF**). Finally, the full-matrix refinements geometric constraints were applied to partial occupancy atoms, and anisotropic displacement parameters were assigned to full occupancy atoms; in (**3**) a common isotropic displacement parameter was applied to all O- and C-atoms to reduce the number of least-squares parameters, and the Friedel pairs in the data were merged using MERG 3.

CCDC reference numbers 766941 (**1**), 766942 (**2**), 799031 (**3**), 799032 (**4**), 799033 (**5**), 799034 (**6**), and 799035 (**7**).

Results and Discussion

Synthesis and Characterization of 2−7. It has been reported previously that the 1:1 or 2:1 stoichiometric reactions of $[KTi_2(OR)_9]$ (**A**) in benzene with a series of divalent metal salts $[MCl_2]$ give complexes in which the dinuclear $[Ti_2(OR)_9]^-$ anion is transferred *intact* to the metal ions.[26,27] In particular, the trinuclear Co^{II} complex $[Ti_2(OEt)_9(CoCl)]$, whose structure is assumed to be related to the structurally characterized complex $[Ti_2(O^iPr)_9(CuCl)]$,[28] was prepared via the reaction of $[KTi_2(OEt)_9]$ with $CoCl_2$ (Scheme 1a).[26]

We found, however, that the 1:1 or 2:1 reactions of $[KTi_2(OEt)_9]$ (**A**) with $CoCl_2$ in toluene at reflux did not afford the expected crystalline products $[Ti_2(OEt)_9(CoCl)]$ (monosubstituted) or $[\{Ti_2(OEt)_9\}_2Co]$ (disubstituted) after workup. Instead, we were only ever able to isolate a small amount of the octanuclear cage $[Ti_7O_5(OEt)_{19}(CoCl)]$ (**1**) (Scheme 1b) (see Figure 1 for the solid-state structure of **1**), mixed with crystals of the starting material $[KTi_2(OEt)_9]_\infty$. It has been shown previously that the neutral cage $[Ti_7O_4(OEt)_{20}]$ (which is structurally related to **1**) can be obtained via thermolysis of neat $[Ti(OEt)_4]$ in an autoclave, with the formation of the oxo anions being thought to occur from cleavage of EtO groups under these conditions.[29] We reasoned that thermolysis in the presence of $CoCl_2$ may result in a higher yielding route to **1**. However, the subsequent solvothermal reaction of $[Ti(OEt)_4]$ with $CoCl_2$, using a range of stoichiometries of $Ti(OEt)_4$:$CoCl_2$ in ethanol, actually gave the cage $[Ti_4O(OEt)_{15}(CoCl)]$ (**2**) which we have communicated earlier.[12] The highest yield of **2** was obtained using a 16:1 stoichiometry of $Ti(OEt)_4$ to $CoCl_2$ (respectively) with dry ethanol as solvent at 100 °C for 14 days. Evaporation of the volatile products and crystallization from dry toluene gave a 72% yield of **2** (based on $CoCl_2$ supplied). In fact, we have now found that even given a reaction time of 1 day at 150 °C a similar high yield of **2** is obtained.

Scheme 2. Formation of Compounds **2**−**7**[a]

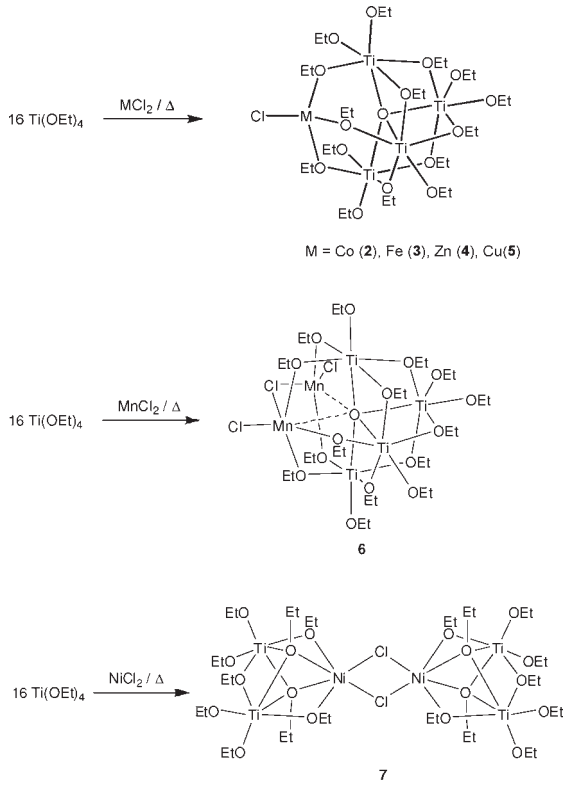

[a] Formation via solvothermal reaction thermolysis of excess $[Ti(OEt)_4]$ with $M^{II}Cl_2$. Note that the arrangement around M (= Cu) in **5** slightly differs to the diagram due to Jahn−Teller distortion.

In further studies we have now explored the solvothermal reactions of $Ti(OEt)_4$ with other metal dichlorides ($M^{II}Cl_2$; M = Zn, Fe, Cu, Mn, Ni) using a variety of Ti:M stoichiometric ratios and reaction temperatures (Scheme 2) (see Experimental Section). Using this method the new compounds $[Ti_4O(OEt)_{15}(MCl)]$ [M = Zn (**3**), Fe (**4**), Cu(**5**)], $[Ti_4(OEt)_{15}(Mn_2Cl_3)]$ (**6**), and $[Ti_2(OEt)_9(NiCl)]_2$ (**7**) have been obtained in crystalline form in moderate to good yields (30−68%). The complex **4** was also obtained using iron(III) chloride instead of iron(II) chloride. To obtain crystalline heterometallic cages containing Cu^{II}, it was found that the temperature had to be lowered to 100 °C, otherwise only a brown immiscible liquid was formed.

All of the compounds **2**−**7** were characterized initially by IR, ^1H, and ^{13}C NMR spectroscopy as well as by elemental analysis. The interpretation of the NMR spectra was hampered by the presence of paramagnetic metal ions in **2** and **4**−**7**. The ^1H and ^{13}C NMR spectra of **2** and **4**−**7** exhibit marked paramagnetic shifting and broadening of the resonances, all showing overlapping resonances around $\delta \sim 4.6$ and ~ 1.4 for the methylene

(26) Agrawal, N.; Singh, A. *J. Indian Chem. Soc.* **2007**, *84*, 532.
(27) Agrawal, N.; Singh, A. *Transition Met. Chem.* **2007**, *32*, 615.
(28) Veith, M.; Mathur, S.; Huch, V. *Inorg. Chem.* **1997**, *36*, 2391.
(29) Steunou, N.; Dromzee, Y.; Robert, F.; Sanchez, C. *Mater. Res. Soc. Symp. Proc.* **1996**, *435*, 487.

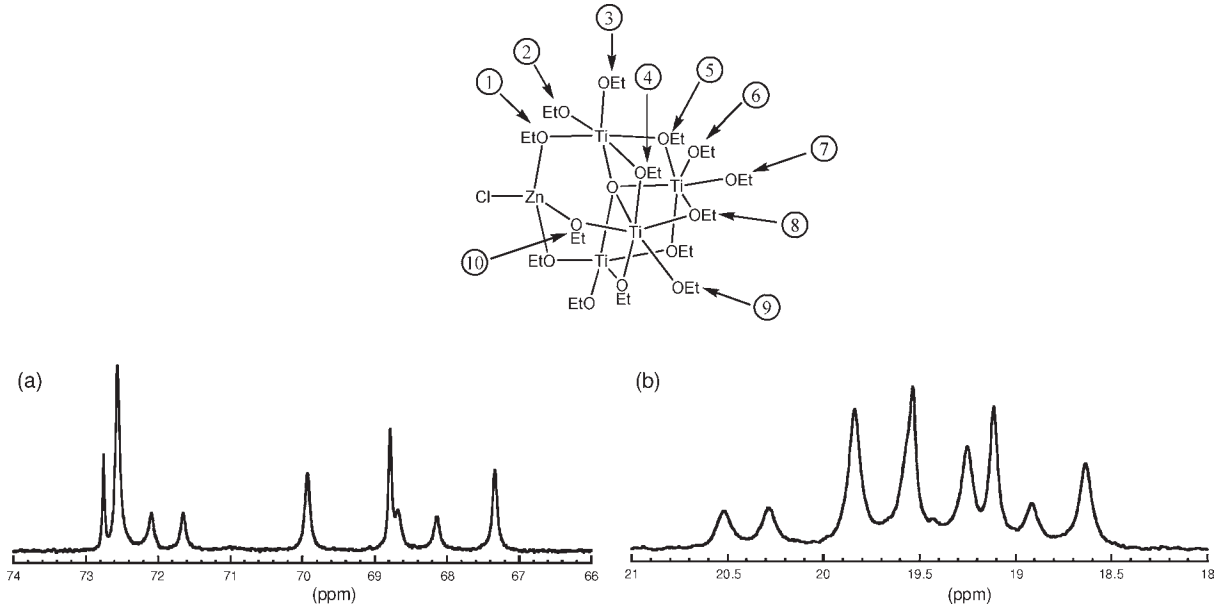

Figure 3. The ^{13}C NMR spectrum of $[Ti_4O(OEt)_{15}(ZnCl)]$ cage **3** in the (a) $-OCH_2-$ and (b) CH_3 resonance regions.

($-OCH_2-$) and methyl (CH_3) groups, respectively. Integration of the spectra proved impossible. The ^{13}C NMR spectra show collections of resonances at $\delta \sim 70$ and ~ 20 for these groups, respectively. However, the presence of the diamagnetic Zn^{2+} in the cage **3** results in a much sharper series of overlapping resonances for the methylene and methyl groups. The ^{13}C NMR spectrum is particularly diagnostic, showing nine distinct resonances in both the methylene and methyl regions (Figure 3). It should be noted in this regard that the apparent single resonance at δ 19.3 in the CH_3 region has a shoulder and is actually two resonances. Assuming virtual mirror symmetry in the molecule of **3**, there should in theory be 10 distinct Et environments [i.e., with the virtual plane of symmetry Ti(4)Ti(3)O(1)M in the solid-state structure shown in Figure 2 (see also the insert to Figure 3)]. The analysis of $^{13}C-^{1}H$ HSQC 2D and $^{1}H-^{1}H$ COSY 2D spectra (results shown in Supporting Information) shows that the resonances at δ 72.6 (CH_2 region) and δ 19.6 (CH_3 region) in both cases consist of two coincident signals, finally confirming the presence of 10 environments for the methylene and methyl carbons. It can therefore be concluded that the solution structure of **3** is similar to that later determined in the solid state with little or no dissociation or fragmentation occurring. We next attempted to broadly assign the resonances found for the EtO groups in the ^{13}C NMR spectrum of **3** to terminal or μ_2-environments on the basis of the methodology which has been applied previously to the cage $[Ti_{16}O_{16}(OEt)_{32}]$, by measurement of the relaxation times T_1 in the methylene region.[6] For this Ti_{16} cage, short T_1 relaxation times (ca. 0.1 s) have been found for the methylene groups in μ_2-OEt environments and long T_1 relaxation times (ca. 0.4−0.9 s) are found for methylene groups in terminal EtO groups. However, disappointingly in the case of **3** T_1 relaxation times were found to be between 0.56 and 0.87 s, which did not allow unambiguous assignment of the type of EtO groups present.

UV−vis spectroscopy of cages **2**−**7** in solution shows different optical properties depending on the atomic

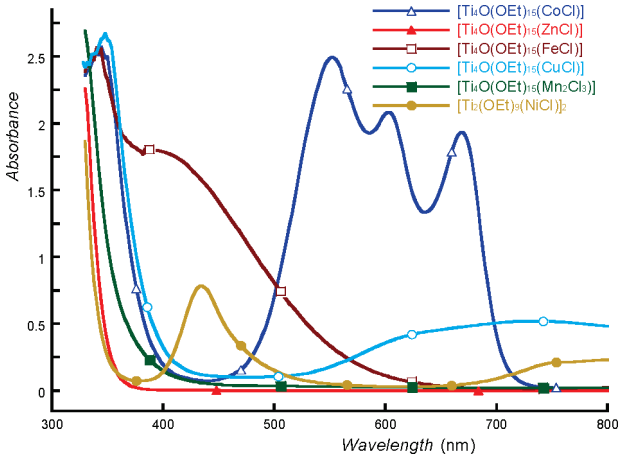

Figure 4. UV−vis absorbance of the cages **2**−**5** and **7** in toluene and **6** in THF (concentration of 10 mM for all).

composition (Figure 4). They all have an absorption edge in the UVA region (315−400 nm) ascribed in the case of **2**−**6** to the Ti_xO_y core in the compounds. It is noteworthy in this respect that **7** (not possessing an oxo core) has the most blue-shifted absorption edge. The previously reported Co^{II} compound **2** shows absorption bands centered at 552, 602, and 668 nm corresponding to $^4A_2 \rightarrow {}^4T$ transitions expected for tetrahedral Co^{II}. The Zn cage **3** is the most transparent complex, having no absorption in the visible area (as expected for a closed shell d^{10} electronic configuration) and minimal absorption in the UVA region. The cage **4**, containing tetrahedral Fe(II), exhibits a broad absorption in the visible region. This absorption is of too high energy to be a simple $^5E_2 \rightarrow {}^5T_2$ transition and most likely arises from loss of degeneracy of the $^5T_2$ state.[30] Cage **5**, containing four-coordinate Cu(II), shows a broad absorption band in the red region, typical of tetrahedral Cu(II) coordination compounds ($^2T \rightarrow {}^2E$).[31]

(30) Quagliano, J. V.; Banerjee, A. K.; Goedken, V. L.; Vallarino, L. M. *J. Am. Chem. Soc.* **1970**, *92*, 482.

Table 1. Crystal Data and Structure Refinement Parameters for the New Compounds **3**−**7**

compound	**3**	**4**	**5**	**6**·(**1/2EtOH**)·(**1/2THF**)	**7**
formula	$C_{30}H_{75}ClZnO_{16}Ti_4$	$C_{30}H_{75}ClFeO_{16}Ti_4$	$C_{30}H_{75}ClCuO_{16}Ti_4$	$C_{33}H_{82}Cl_3Mn_2O_{17}Ti_4$	$C_{36}H_{90}Cl_2Ni_2O_{18}Ti_4$
M	984.32	974.80	982.49	1158.82	1191.00
cryst. size (mm)	0.16 × 0.12 × 0.07	0.35 × 0.32 × 0.30	0.18 × 0.16 × 0.05	0.25 × 0.12 × 0.10	0.16 × 0.16 × 0.05
color	colorless	brown	light blue	pale yellow	pale yellow
cryst. system	monoclinic	monoclinic	triclinic	monoclinic	orthorhombic
space group	*Cc*	*Cc*	*P*-1	*P*2(1)/*c*	*Pbcn*
a (Å)	21.9921(4)	21.9579(3)	11.6537(3)	11.7243(1)	15.1091(4)
b (Å)	10.8819(2)	10.9435(2)	11.8104(3)	20.4895(3)	23.5591(9)
c (Å)	22.4773(5)	22.4042(4)	19.9739(8)	23.5632(3)	16.4439(4)
α (°)	90.000	90.000	87.120(2)	90	90
β (°)	118.842(1)	118.512(1)	80.609(2)	92.182(1)	90
γ (°)	90.000	90.000	60.787(2)	90	90
V (Å^3)	4711.90(16)	4730.7(2)	2365.91(13)	5656.37(12)	5853.3(3)
Z	4	4	2	4	4
d_{calc} (g cm^{-3})	1.388	1.369	1.379	1.361	1.352
μ (mm^{-1})	1.264	1.059	1.201	1.167	1.298
F(000)	2072	2056	1034	2420	2512
θ range (°)	3.60−27.86	3.59 to 27.83	3.53−26.38	3.54−25.00	3.66−22.98
reflections collected	8576	21 345	30 198	56 607	15 254
independent refl. [R_{int}]	2707 [0.0323]	5568 [0.0397]	9494 [0.0576]	9906 [0.0392]	4047 [0.0534]
Final R_1 and wR_2 [$I/s(I) > 2$]	0.0674 and 0.2041	0.0398 and 0.1067	0.0770 and0.1789	0.0680 and 0.1818	0.0494 and 0.1118
R_1 and wR_2 (all data)	0.0788 and 0.2111	0.0505 and 0.1121	0.1174 and0.2193	0.0886 and 0.1923	0.0818 and 0.1289
T (°C)	180(2)	180(2)	180(2)	180(2)	270(2)

Although Jahn−Teller compression of the tetrahedral geometry of the Cu^{2+} ion is observed in the solid-state structure of **5**, the broadness of the absorption in the visible region presumably masks any resulting splitting of this band. In the cage **6**, containing five-coordinate Mn(II), it is not possible to identify many, if any, of the spin-forbidden low-intensity d−d transitions because the UV absorption that tails into the visible region obscures them; this is consistent with previous observations in the literature.[31] Finally, the most blue-shifted UV absorption edge corresponds to the Ni complex **7**, which does not contain an oxo core. This cage, containing octahedral Ni(II), shows two absorption bands in the visible region at ca. 430 and 800 nm, corresponding to two of the three spin-allowed transitions [$^3A_{2\,g} \rightarrow {}^3T_{1\,g}$(P) and to $^3A_{2\,g} \rightarrow {}^3T_{1\,g}$(F), respectively].[31]

X-ray Structures of 3−7. The low-temperature X-ray structures of the new compounds **3**−**7** were obtained. Details of the data collections and structural refinements are summarized in Table 1 (see Experimental Section).

$[Ti_4O(OEt)_{15}(ZnCl)]$ (**3**) and $[Ti_4O(OEt)_{15}(FeCl)]$ (**4**) are isostructural with the previously reported compound $[Ti_4O(OEt)_{15}(CoCl)]$ (**2**) (Figure 2). Their cores are heterometallic cages of virtual C_s symmetry, each containing a trigonal bipyramidal Ti_4M core arrangement (M = Zn or Fe), composed of a tetrahedral $Ti_4(\mu_4\text{-O})$ fragment capped at one of the faces by a M^{II} center. Alternatively, these structures can be regarded as ion pairs of the $[Ti_4O(OEt)_{15}]^-$ anion with the $[MCl]^+$ cation fragments. The M^{2+} ions are bonded to the cage by three μ_2-OEt bridges [Co−O 1.956(3)−1.969(3) Å range in **2**; Fe−O 1.978(4)−1.998(3) Å range in **3**; and Zn−O 1.944(3)−1.961(10) Å range in **4**]. The pseudotetrahedral geometries of these M^{2+} ions are completed by bonding to a Cl center, directed exo to the core of the cage. Although there is a potential for longer range M···O bonding to the μ_4-O atoms within the $Ti_4(\mu_4\text{-O})$ units of **2**−**4** [Co···O 2.936(3) Å in **2**; Fe···O 2.938(4) Å in **3**; and Zn···O 3.062(13) Å in **4**], these interactions are at best weak. In the Ti_7Co cage **1** (Figure 1) the nominally μ_5-O atom is distorted significantly toward octahedral, and there is a much shorter M···O contact [2.599(2) Å], suggesting a more significant interaction. The type of arrangement found in **2**−**4** is unique in titanium oxo cages.[32]

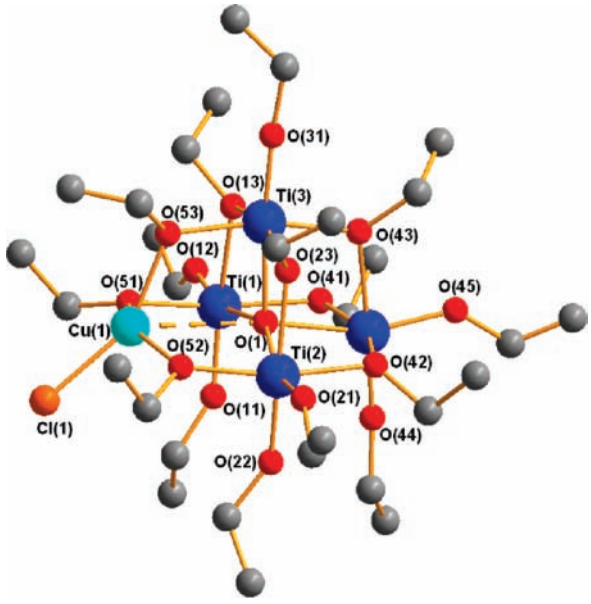

Figure 5. Structure of the heterometallic complex $[Ti_4O(OEt)_{15}(CuCl)]$ (**5**). H-atoms and the minor components of disorder in EtO groups are omitted for clarity. Selected bond lengths (Å) and angles (°): Ti−OEt-(terminal) range 1.761(4)−1.816(5), Ti−(μ_2-OEt) range 1.951(4)−2.093(4), Ti−μ_2-O(51, 52, 53) range 1.952(5)−1.980(4), Ti−O(1) range 2.055-(4)−2.164(4), Cu(1)−Cl(1) 2.213(3), Cu(1)−μ_2-O(51,52,53) range 1.930-(5)−1.981(4), Cu(1)···O(1) 2.771(3), Ti−O(1)−Ti range 96.8(2)−153.5(2), O(52)−Cu(1)−O(51) 146.4(2), O(52)−Cu(1)−O(53) 90.8(2), O(51)−Cu(1)−O(53) 90.3(2), O(52)−Cu(1)−Cl(1) 97.4(2), O(51)−Cu-(1)−Cl(1) 98.3(2), O(53)−Cu(1)−Cl(1) 150.0(1), Ti−(μ_2-OEt)−Ti range 104.1(2)−106.9(2), Cu(1)−O−Ti range 112.5(2)−113.9(2).

$[Ti_4O(OEt)_{15}(CuCl)]$ (**5**) (Figure 5) shows a similar structure to the previous cages **2**−**4**. However, there is a noticeable Jahn−Teller compression of the tetrahedral

(31) Lever, A. B. P. In *Inorganic Electronic Spectroscopy*, 2nd ed.; Elsevier: Amsterdam, The Netherlands, 1984.

Table 2. Selected Bond Lengths and Angles at the Metal Ions and Interstitial O Atoms of Cages **2**−**6**

compound	2	3	4	5	6
formula	$C_{30}H_{75}ClCoO_{16}Ti_4$	$C_{30}H_{75}ClZnO_{16}Ti_4$	$C_{30}H_{75}ClFeO_{16}Ti_4$	$C_{30}H_{75}ClCuO_{16}Ti_4$	$C_{30}H_{75}C_{l3}Mn_2O_{16}Ti_4$
M−O(1) (Å)	2.934(3)	3.062(12)	2.938(4)	2.771(3)	2.845(6)/2.826(6)
Ti(1)−O(1)−Ti(2) (°)	149.8(1)	149.0(3)	150.7(1)	153.5(2)	163.7(3)

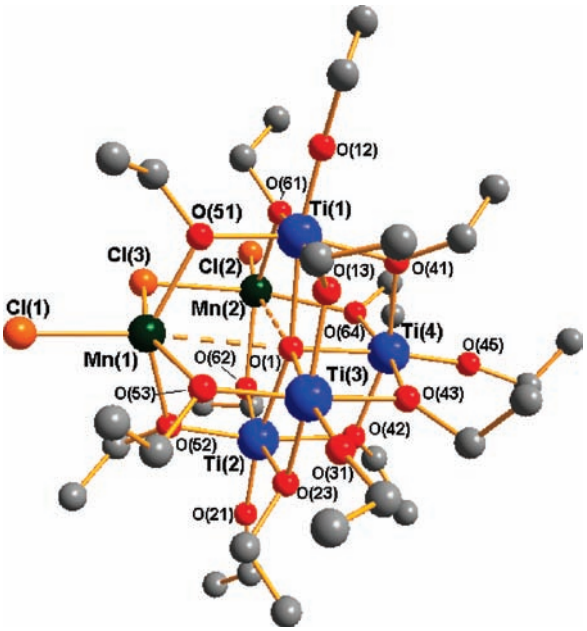

Figure 6. Structure of the heterometallic complex $[Ti_4O(OEt)_{15}(Mn_2Cl_3)]$ (**6**). H-atoms and the minor disorder components in the EtO groups are omitted for clarity. Selected bond lengths (Å) and angles (°): Ti−OEt(terminal) range 1.753(6)−1.763(4), Ti−(μ_2-OEt) range 1.975(4)−2.039(3), Ti−μ_2-O(51, 52, 53, 61, 62, 64) range 1.898(4)−1.920(4), Ti−O(1) range 2.106(3)−2.239(3), Mn−Cl(1,2) range 2.352(2)−2.366(2), Mn−Cl(3) range 2.493(3)−2.520(2), Mn−μ_2-O range 2.136(4)−2.224(3), Mn···O(1) range 2.832(3)−2.849(4), (Ti,Mn)−O(1)−(Ti,Mn) range 83.6(1)−172.7(2), O−Mn−O range 83.3(1)−141.6(1), Cl(1,2)−Mn−(O, Cl(3)) range 100.1(1)−110.1(1), Ti−(μ_2-OEt)−Ti range 106.1(2)−106.7(2), Mn−(μ_2-OEt)−Ti range 114.3(2)−116.5(2). The atomic labels have been modified from those in the CIF file for consistency.

geometry around Cu^{2+}. In the cages **2**−**4**, the metal is in pseudotetrahedral geometry, with Cl(1)−M−O angles in the range 106.6(1)−117.7(5)°, i.e., around the ideal 109.5° angle of a regular tetrahedron. However, in cage **5** the Cl(1)−Cu(1)−O angles are 97.4(2), 98.3(2), and 150.0(1)°. This distortion is unlikely to result from steric factors since no such extreme distortion of the Co^{2+}, Zn^{2+}, and Fe^{2+} ions is found in **2**−**4** (these ions ranging from being larger and smaller than Cu^{2+}). The presence of electronically based Jahn−Teller distortion is further supported by the magnitude of the angles around Cu^{2+} in cage **5** being very similar to those found in the tetrahedral Cu^{II} complex 1,2-bis(diphenylphosphineoxido)ethane copper(II) chloride, which is also reported to possess Jahn−Teller distortion.[33] The presence of Jahn−Teller distortion in the Cu^{2+} promotes the interaction between this ion and the central oxo atom [O(1)] of the cage: the Cu···O(1) in **5** is significantly shorter, at 2.771(3) Å than the corresponding M···O(1) contacts in **2**−**4** (see Table 2). In addition, the Ti(1)−O(1)−Ti(2) angle in **5** is more than 2.8° wider than those found for

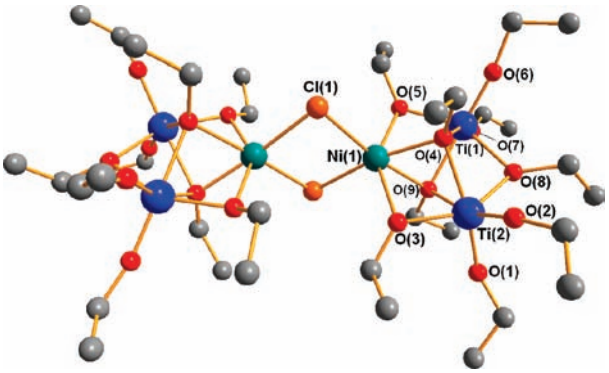

Figure 7. Structure of the heterometallic complex $[Ti_2(OEt)_9(NiCl)]_2$ (**7**) which has crystallographic C_2 symmetry. H-atoms and the minor components of disorder in EtO groups are omitted for clarity. Selected bond lengths (Å) and angles (°): Ti−OEt(terminal) range 1.749(4)−1.779(4), Ti−(μ_2-OEt) range 1.918(4)−2.043(4), Ti−(μ_3-OEt) range 2.104(3)−2.131(4), Ni−(μ_2-OEt) range 2.113(4)−2.170(4), Ni−(μ_3-OEt) 2.038(3), Ni−Cl range 2.345(2)−2.367(1).

the other cages (Table 2). It is worthwhile noting also that the apparently greater strength of the Cu···O(1) interaction in **5** is in-line with the expected effects of crystal field and Z_{eff} on the bond energies (i.e., Irving−Williams order).[34]

The solid structure of **6** is closely related to that of **2**−**5**. However, in **6** the coordinated $(MCl)^+$ unit is replaced by a $[ClMn(\mu\text{-}Cl)MnCl]^+$ cation unit, giving a hexanuclear arrangement containing an octahedral Mn_2Ti_4 core (Figure 6). Six EtO groups of the $[Ti_4O(OEt)_{15}]^-$ anion are involved in the coordination of the $[ClMn(\mu\text{-}Cl)MnCl]^+$ unit, with each of the Mn^{2+} ions being bonded to three different μ-OEt groups and two Cl^- ions. Unlike the $Ti_4(\mu_4\text{-}O)$ cores of **2**−**4**, the interstitial O atom of **6** [O(1)] is noticeably distorted toward pseudo-octahedral, suggesting that weak interactions to the Mn^{2+} ions are present [Mn···O range 2.832(3)−2.849(4) Å]. These M···O interactions are slighty shorter than those found in structurally related cages **2**−**4** (all > 2.93 Å).

A completely different outcome to the thermolysis reaction is seen in the structure of the heterometallic Ni_2Ti_4 compound **6** (Figure 7). The structure of **7** (with two-fold symmetry) is composed of two, symmetry-related $Ti_2(OEt)_9(NiCl)$ monomer units which are associated via a central $Ni_2(\mu\text{-}Cl)_2$ ring. Notably, there are no oxo anions within the $[Ti_2(OEt)_9]^-$ anion of **7**, in contrast to the formation of the $[Ti_4O(OEt)_{15}]^-$ anion in **2**−**6**. The compound **7** has been synthesized previously using the metal-exchange reaction of $[KTi_2(OEt)_9]$ and $[NiCl_2]$[35] but was only characterized by elemental analysis and IR spectroscopy. A similar $[Ti_2(OR)_9]^-$ anion has, however, been seen previously in the solid-state structure of the analogous Cu^{II}/O^iPr compound $[Ti_2(O^iPr)_9(CuCl)]$.[28]

(32) Johnson, B. F. G.; Klunduk, M. C.; O'Connell, T. J.; McIntosh, C.; Ridland, J. *J. Chem. Soc., Dalton Trans.* **2001**, 1553.
(33) Mathew, M.; Palenik, G. J. *Can. J. Chem.* **1969**, *47*, 1093.
(34) Irving, H.; Williams, R. J. P. *J. Chem. Soc.* **1953**, 3192.
(35) Agrawal, N.; Singh, A. *Indian J. Chem., Sect. A: Inorg., Bio-inorg., Phys., Theor. Anal. Chem.* **2007**, *46a*, 1938.

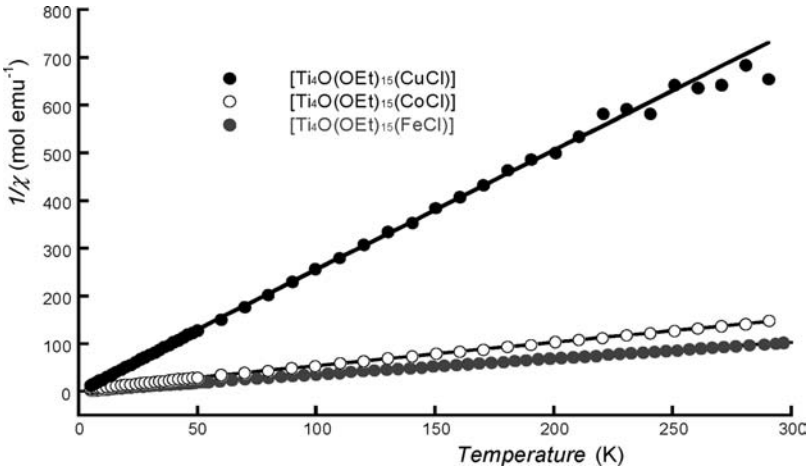

Figure 8. Temperature dependence of the inverse susceptibility of the mononuclear compounds **2**, **4**, and **5** revealing Curie−Weiss behavior associated with spin-only ions; compound **2** ○ (C = 2.05 emu K mol^{-1}, θ = −11 K); compound **4** ● (C = 2.99 emu K mol^{-1}, θ = −11 K); and compound **5** ● (C = 0.40 emu K mol^{-1}, θ = −2 K).

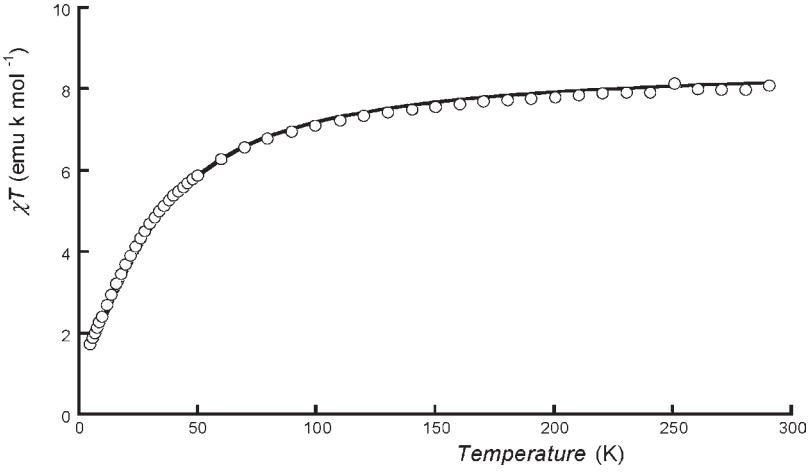

Figure 9. Temperature dependence of χT for the hexanuclear complex **6**. Solid line represents the fit to the model with g = 1.99 and J/k = −3.4 K.

Magnetic Measurements. Variable-temperature magnetic measurements were focused on understanding the behavior of the oxo complexes (**2** and **4**−**6**). Complexes **2**, **4**, and **5**, containing one transition-metal ion, obey Curie−Weiss-type behavior down to low temperature, consistent with the presence of isolated spin-only ions (Figure 8). The cobalt(II) compound **2** has a Curie constant C = 2.05 emu K mol^{-1} consistent with a $S = {}^3/_2$ ion with $g \sim 2.09$, expected for the ^{4}A state of the pseudotetrahedral Co^{II} ion. The iron(II) complex **4** has C = 2.99 emu K mol^{-1} consistent with a S = 2 ion with $g \sim 2$ (3.00 emu K mol^{-1}), expected for the ^{5}E state of the pseudotetrahedral Fe^{II} ion. The copper(II) complex **5** exhibits a C = 0.40 emu K mol^{-1} consistent with a S = 1/2 ion with g = 2.07. All three compounds exhibit some deviation from pure Curie behavior consistent with the presence of some zero-field splitting of the $S = {}^3/_2$ or 2 terms for **2** and **4**, respectively, and/or weak through-space dipolar interactions (**2**, **4**, and **5**).

The manganese(II) complex (**6**) exhibits Curie−Weiss behavior in the region 20−300 K with C = 8.66 emu K mol^{-1} per cage, consistent with two $S = {}^5/_2$ ions with g = 1.99 (Figure 9). The Weiss constant (−21.9 K) is consistent with antiferromagnetic exchange interactions between the two $S = {}^5/_2$ ions. A first estimate of the exchange coupling between the two ions can be extracted from the mean-field approximation (eq 1) yielding $J/k \sim -3.8$ K:

$$\theta = -2zJS(S+1)/3k \quad (1)$$

The magnetic behavior of **6** was further modeled using an isotropic exchange Hamiltonian:

$$H = 2J\hat{s}_1\hat{s}_2 \quad (2)$$

The solution to this Hamiltonian yields a series of spin states for the complex ranging from S_T = 0 to 5 and the magnetic susceptibility is

$$\begin{aligned} x = (Ng^2\beta^2/3kT)\cdot[(330e^{25J/2kT} + 180e^{5J/2kT} \\ + 84e^{-11J/2kT} + 30e^{-23J/2kT} \\ + 6e^{-31J/2kT})/(11e^{25J/2kT} + 9e^{5J/2kT} \\ +7e^{-11J/2kT} + 5e^{-23J/2kT} \\ +3e^{-31J/2kT} + e^{-35J/2kT})] \end{aligned} \quad (3)$$

A fit to the data (Figure 9) yielded $g = 1.99$ and $J/k = -3.4$ K, in good agreement with the estimates made using the mean-field approximation.

The nickel cage **7** obeys Curie−Weiss behavior with $C = 2.60$ emu K mol^{-1} consistent with two $S = 1$ ions and $g = 2.28$. The Weiss constant ($\theta = +1.9$ K) reflects weak ferromagnetic interactions between Ni^{II} ions. An estimate of the exchange coupling between ions was similarly estimated from the mean-field approximation (eq 1), yielding $J/k = +1.4$ K, i.e., ferromagnetic. However, we were unable to model the low-temperature behavior of the compound using a dimer model owing to the presence of persistent contamination, probably traces of $NiCl_2$.

Conclusions

In conclusion, we have demonstrated a simple route to obtain a whole family of heterometallic metal(II) titanium oxo alkoxo cages, involving solvothermal reactions in dry ethanol of [Ti(OEt)$_4$] with metal dichlorides ($M^{II}Cl_2$, M = Co, Zn, Fe, Cu, and Mn). The formation of heterometallic transition-metal/titanium oxo cages in this way represents a new direction in this area which has the potential to uncover a large area of new structural chemistry. The products of these reactions also provide well-defined new molecular precursors for a number of applications, such as heterometallic building blocks for advanced hybrid materials as well as the use of controlled hydrolysis in the formation of transition-metal doped, bulk TiO_2 itself. We are currently investigating these applications, and work in this area will be reported in due course.

Acknowledgment. We thank the EPSRC for funding this work (DSW and PDRA for S.E., grant number EP/F00253X/1); Dr. J. E. Davies (Cambridge) for collecting crystallographic data, and Dr. A. Wheatley and Dr. P. T. Wood for useful scientific discussions.

Supporting Information Available: Crystallographic data of clusters **1**−**7** in CIF format and $^{13}C-^{1}H$ HSQC 2D and $^{1}H-^{1}H$ COSY 2D spectra. This material is available free of charge via the Internet at http://pubs.acs.org.